VYSOKÉ UČENÍ TECHNICKÉ V BRNĚ
BRNO UNIVERSITY OF TECHNOLOGY

FAKULTA CHEMICKÁ
ÚSTAV CHEMIE MATERIÁLŮ

FACULTY OF CHEMISTRY
INSTITUTE OF MATERIALS SCIENCE

STUDY OF THIN-FILM SURFACES

AUTOREFERÁT DESERTAČNÍ PRÁCE
PHD THESIS

AUTOR PRÁCE
AUTHOR

ING. RUTUL RAJENDRA TRIVEDI

BRNO 2010

VYSOKÉ UČENÍ TECHNICKÉ V BRNĚ
FAKULTA CHEMICKÁ
ÚSTAV CHEMIE MATERIÁLŮ

Ing. Rutul Rajendra Trivedi

STUDY OF THIN-FILM SURFACES

STUDIUM POVRCHU TENKOVRSTVÝCH MATERIÁLŮ

AUTOREFERÁT Ph.D. THESIS

Školitel: prof. RNDr. VLADIMÍR ČECH, Ph.D.

Oponenti: prof. RNDr. Tomáš Šikola, CSc.
RNDr. Antonín Fejfar, CSc.
RNDr. Petr Klapetek, Ph.D.

Datum obhajoby: Leden 2011

BRNO 2010

ABSTRACT

The doctoral thesis deals with the study of surface properties of single-layer and multilayer thin films deposited from of vinyltriethoxysilane and tetravinylsilane monomers. It also deals with adhesion characterization of single layer tetravinylsilane films. The plasma polymerized thin films were prepared under steady-state deposition conditions on polished silicon wafers using plasma-enhanced chemical vapor deposition. The surface properties of the films were been characterized by different scanning probe microscopy methods and nanoindentation techniques such as conventional depth-sensing nanoindentation and load-partial-unload (cyclic) nanoindentation. While, the nanoscratch test was used to characterize the film adhesion properties.

Single layer films prepared at different deposition conditions were characterized with respect to surface morphology and mechanical properties (Young's modulus and hardness). The results of surface morphology, grain analysis, nanoindentation, finite elemental analysis and modulus mapping helped to know the hybrid nature of single layer films that were deposited at higher powers of RF-discharge. A novel approach was used in surface characterization of multilayer film by scanning probe microscopy and nanoindentation. The adhesion behavior of plasma polymer films of different mechanical properties and film thickness were analyzed by normal and lateral forces, friction coefficient, and scratch images obtained by atomic force microscopy.

ABSTRAKT

Disertační práce se zabývá studiem povrchových vlastností jedno a vícevrstvých filmů deponovaných z vinyltriethoxysilanových a tetravinylsilanových monomerů. Zabývá se také charakterizací adheze jednovrstvých filmů z tetravinylsilanu. Plazmaticky polymerizované tenké vrstvy byly připraveny na leštěných křemíkových substrátech pomocí plazmové depozice z plynné fáze za ustálených podmínek. Povrchové vlastnosti vrstev byly charakterizovány pomocí různých metod rastrovací sondové mikroskopie a nanoindentačních technik jako je konvenční a cyklická nanoindentace. Vrypový test byl použit pro charakterizaci vlastností adheze vrstev.

Jednovrstvé filmy připravené za různých depozičních podmínek byly charakterizovány s ohledem na povrchové morfologie a mechanické vlastností (modul pružnosti, tvrdost). Výsledky morfologie povrchu, analýzy zrn, nanoindentace, analýzy konečných prvků a modulů mapování pomohly rozlišit hybridní charakter filmů, které byly deponovány při vyšších výkonech RF-výboje. Nový přístup byl použit v povrchové charakterizaci vícevrstvého filmu pomocí rastrovací sondové mikroskopie a nanoindentace. Adhezívní chování plazmaticky polymerizovaných vrstev různých mechanických vlastností a tloušťek bylo analyzováno pomocí normálních a laterálních sil, koeficientu tření, a snímků vrypů získaných pomocí mikroskopie atomárních sil.

INDEX

1 INTRODUCTION 4

2 THEORETICAL BACKGROUND 5
2.1 Plasma …… 5
2.2 Plasma-enhanced chemical vapor deposition(PECVD)……..... 5
2.3 Scanning Probe Microscopy……... 6
2.3.1 Basic concept of SPM……..... 6
2.3.2 Atomic force microscopy.……. 7
2.4 Nanoindentation…….. 8

3 EXPERIMENT 9
3.1 Scanning Probe Microscope..... 9
3.1.1 Scanning probe microscope basic setup..... 9
3.2 Nanoindentation Technique..... 10

4. RESULTS AND DISCUSSIONS 12
4.1 Single layer film…….. 12
4.1.1 Surface analysis by AFM…….. 12
4.1.2 Mechanical properties..... 13
Set 1 (drift rate ≤ 0.5 nm/s)..... 14
Set 2 (drift rate ≤ 0.05 nm/s)..... 14
4.2 Hybrid film…….. 17
4.2.1 Surface morphology analysis by AFM……. 18
4.2.2 Mechanical properties……... 19
4.2.3 Surface analysis by atomic force acoustic microscopy……. 21
4.3 Adhesion test……... 22
4.3.1 Study of effect of different scratch speed on adhesion data….. 22
4.3.2 Reproducibility of adhesion data …… 23
4.3.3 Effect of different film thickness on adhesion failures……. 24
4.3.4 Effect of thin films of different mechanical properties on adhesion behavior…….. 26
4.4 Multilayer film…… 27
4.4.1 Surface analysis of thin films in normal direction…… 27
4.4.2 Multilayer film analysis by AFM and nanoindentation ……... 28
4.4.3 Multilayer film analysis by LFM ……. 31
4.4.4 Multilayer film analysis by AFAM …….……. 31

CONCLUSION 32

REFERENCES 34

1 INTRODUCTION

Tailoring surfaces by plasma modification and polymerization has proven to be a powerful technology that has revolutionized surface modification and thin film formation. Plasma polymer films have been a key material in many areas, including electronics, magnetic recording media, optical devices, MEMS, protective coatings, etc. In such developments, a good understanding of the surface properties such as the surface morphology and mechanical properties is very important. Recently, scanning probe microscopy (SPM) and nanoindentation have become the most important methods to measure the surface properties of thin films and coatings.

The doctoral thesis is aimed at the application of Scanning Probe Microscopy (SPM) and nanoindentation method on the study of thin films surfaces. The thin films were been prepared by plasma polymerization technique from tetravinylsilane (TVS) and vinyltriethoxysilane (VTES) monomers at the Institute of Materials Chemistry, Brno University of Technology. The prepared films were been characterized by SPM (NT-MDT, Russia) and nanoindentation (Hysitron, USA). Important surface properties such as the surface roughness, surface analysis and mechanical properties were characterized.

In the chapter 2, the theoretical basics are introduced. The text deals with the basic information about plasma, plasma enhanced chemical vapour deposition, Scanning probe microscopy and nanoindentation. Chapter 3 deals with the experimental sets-up of NT-DMT NTegra Prima Scanning Probe Microscopy and Hysitron Triboscope. The obtained results are presented in detail in chapter 4.

2 THEORETICAL BACKGROUND

2.1 Plasma

Generally, there are three states of matter, i.e., solid, liquid or gas. The plasma is considered as being a fourth state of materials, and it is more highly activated than other three states. Plasma is a mixture of electrons, negatively charged particles, positively charged particles, neutral atoms and molecules. To achieve a plasma state, a temperature more than a few thousand centigrade is applied which brings the collision to the level of ionization of atoms. Thus, the plasma state is in an extremely high energy level compared with solid, liquid and gas state.

The energy for the ionization must be input into atoms and the molecules from an external energy source. Normally the electric energy is a convenient source of energy, which helps to bring the ionization of atoms and molecules. For that purpose, a pair of electrodes working in a capacitive coupling manner or inductive coupling manner is placed in the reaction chamber to supply the electric energy in reaction chamber. The controlled plasma state is very helpful to carry out the plasma polymerization reaction of gaseous monomer or surface treatment. There are three essential terms for plasma generation for plasma polymerization: (1) an energy source for the ionization, (2) a vacuum system for maintaining a plasma state, and (3) a reaction chamber.

2.2 Plasma-Enhanced Chemical Vapor Deposition (PECVD)

In PECVD, the plasma polymerization takes place at low temperature and low-pressure plasma conditions. It uses the electrical energy to generate a glow discharge (plasma) in which the energy is transferred into a gas mixture. This transforms the gas mixture into reactive radicals, ions, neutral atoms and molecules, and other highly excited species. Either these atomic and molecular fragments interact with a substrate and, depending on the nature of these interactions, etching or deposition processes occur at the substrate. Since the formation of the reactive and energetic species in the gas phase occurs by collision in the gas phase, the substrate can be maintained at a low temperature.

As mentioned previously, the two most common methods for coupling the electrical energy into a gas discharge in PECVD are capacitive coupling plasma (CCP) or induction as is done with inductively coupled plasma (ICP). The design of PECVD chamber is based on type of energy supply is used. For example, capacitive coupling type of PECVD reactors is mentioned in Fig. 1 [1]. It is a cold wall parallel-plate reactor inside a cylindrical aluminum chamber. The chamber is maintained at low pressure using vacuum pumps, except when loading and unloading wafers. The top plate or electrode is a showerhead through which gases are injected. The wafers are being placed on the bottom of electrode plate. The high side of the RF power supply is connected to the top electrode. The bottom electrode is grounded.

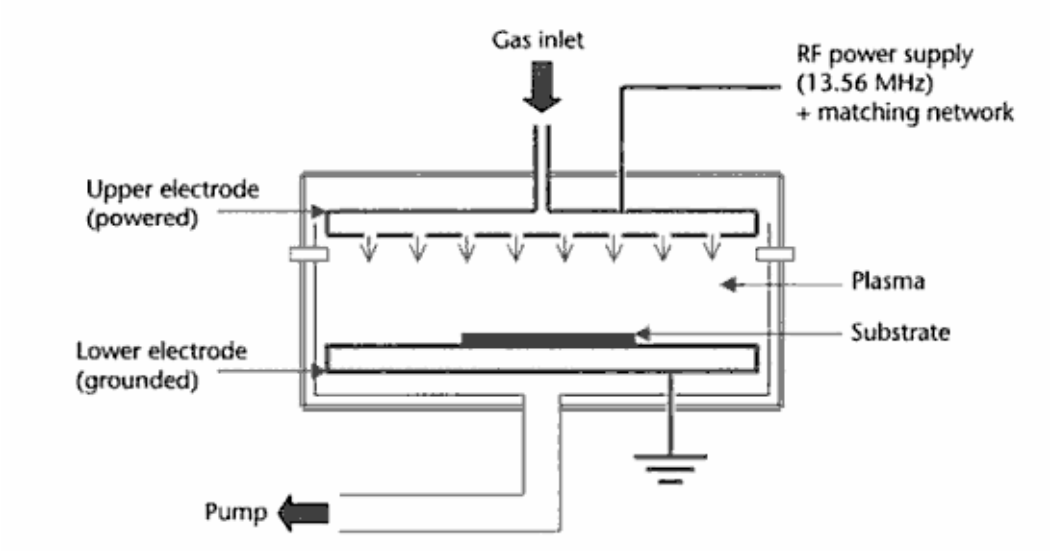

Fig. 1 Schematic diagram of a parallel-plate PECVD reactor [1]

The plasma polymerization in PECVD mostly depends on monomer flow rates, system pressure and discharge power. Some of the desirable properties of PECVD films are having good adhesion, low pinhole density, good step coverage, and uniformity.

2.3 Scanning Probe Microscopy

The revolution in surface analysis was carried out when the scanning tunneling microscope (STM) technique was invented by Dr. Gerd Binning and his colleagues in 1981 at the IBM Zurich Research Laboratory, Switzerland. However, STM technique got some limitations. This limitation of STM, further in 1985 motivated Dr. Binning et al. to develop the Atomic force microscope (AFM) to measure ultra small forces (less than 1 nN) present between the AFM tip surface and sample surface [2]. It was a major breakthrough in the developments of Scanning probe microscopy (SPM) methods, which has given a new vision to the world for studying the surface topographies and normal forces on the micro to nanoscale [3]. With further developments, AFMs have been used for measurements of friction, scratching, wear and adhesion properties [3] and also for the measurement of the elastic/plastic mechanical properties [3].

2.3.1 Basic concept of Scanning Probe Microscope

In Scanning Probe Microscope (SPM), research of a surface structure and its local properties is performed by measuring highly localized tip-sample interactions. The characteristic distance between a tip and a surface of samples in probe microscopes makes about 0.1 – 10 nanometer [4]. Various kinds of tip-sample interactions are laid in the basis of probe microscopy work e.g. electronic tunneling current for Scanning Tunneling Microscopy (STM); force interaction concept used for Atomic Force Microscopy (AFM).

Another important parameter in SPM construction is feedback system (FS). The Feedback system is supervising the distance between a tip and a sample. In existing probe microscopes, the accuracy of keeping the tip-surface distance reaches the value of ~ 0.01 Å [4].

2.3.2 Atomic Force Microscopy

The AFM is the most widely used technique of SPM families because of its experimental flexibility and broad applicability. The AFM can produce very high resolution, 3 D images of sample surfaces. The main working principle in AFM is the measurement of ultra small forces (less than 1 nN) present between an AFM tip and a sample surface. AFMs are capable of investigating the surfaces of both conductive and insulating sample at an atomic scale.

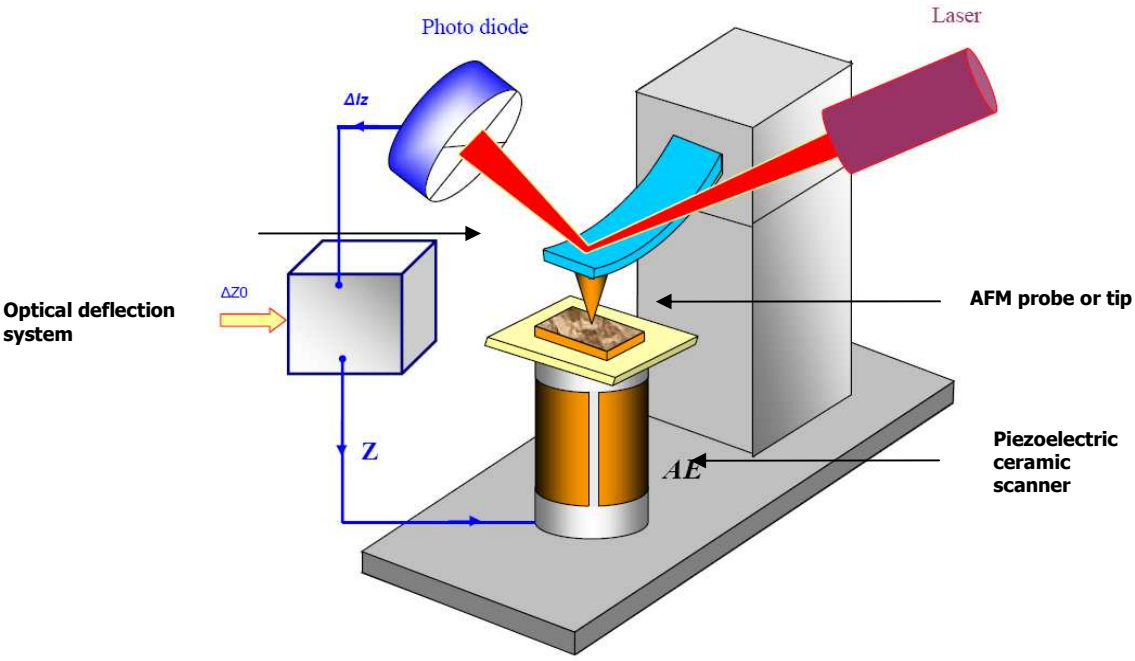

Fig. 2 Schematic diagram of an atomic force microscope

The principle of operation of commercially small sample AFM is shown in Fig 2. The sample is generally smaller than 10 mm x 10 mm. It is mounted on a PZT tube scanner, which controls the movement of sample in *x-y* plane in a raster pattern and to move the sample in *z* direction. A sharp tip at the free end of the cantilever is brought in contact with the sample. The features on the sample surface cause the tip and its cantilever to deflect vertical and lateral directions as the sample is scanned under the tip. A laser beam from a diode is focused on the backside of the cantilever at an angle of 10°. Hence, the reflected beam is captured by the photo diode. The photo diode is connected with the feedback systems. According to the twist and movement of tip cantilever captured by photodiode, the feedback system is used to modulate the voltage applied to the PZT scanner to adjust the height of PZT. The AFM can be used either in static or dynamic mode.

2.4 Nanoindentation

In such developments, a good understanding of the mechanical properties of thin film is essential. It is, however, not a simple undertaking to evaluate the mechanical properties of a thin structure unit at submicron level using conventional testing methods. However, recent years, several techniques have been developed to study the nanomechanical properties of thin films. Among these, nanoindentation is a widely used technique for evaluating nanomechanical properties such as elastic modulus, hardness, and stiffness [5]. Although nanoindentation is an excellent tool, good interpretation of the indentation data is important in order to achieve reliable and repeatable results regarding the mechanical behavior of the thin films.

The two mechanical properties are measured most frequently using load and depth sensing indentation techniques are the elastic modulus, E, and the hardness, H. The Oliver-Pharr [5] method is used for that purpose. There is some limitation regarding the nanoindentation experiment is 10 % rule. According to the rule, the substrate will not influence the nanoindentation experimental data as long as the total indentation depth is less than 10 % of the film thickness. Another important parameter, which influences the nanoindentation experiment, is drift. Some description about drift is mentioned in next paragraphs.

The Berkovich tip is the standard nanoindentation tip, which is widely used for the nanoindentation experiments of thin films. The geometry of a Berkovich tip can be described as a three-sided pyramidal tip with a total included angle of 142.35 degrees and a half-angle of 65.35 degrees. The standard Berkovich tip is available with radius of curvature of 150 nm while the sharper ones are with a radius of curvature of 50 nm. Such pyramidal tips are commonly used in nanoindentation of ceramics, glass, metals, hard polymers, hard & smoothed biomaterial and thin films.

Drift can be due to the vibration or thermal heating (which referred as thermal drift). Thermal drift is caused by the different thermal expansion in the machine or heat generation in the electronic device. Drift can also be referred as the unintentional and unwanted motion to the specimen relative to the indenter, and any unwanted changes in control electronics, during measurement. Drift is especially important while studying time varying phenomenon like creep property of material. Drift can lead to large errors in estimating mechanical properties of specimen.

We have the Hysitron Triboscope instrument with open loop function (i.e. loading without any feedback control) [6], hence, there are more possibilities of introducing the drift errors in indentation experiments. Therefore, it is very important to remove or minimize the drift effect in real indentation experiment. Hence, before every indentation experiment, the drift was monitored and analyzed for preset time (s). This measured drift rate is used to correct the load-displacement data.

3 Experiment

The plasma polymer films used for analyses in this dissertation were deposited from organosilicon monomers (tetravinylsilane and vinlytriethoxysilane) with the help of plasma enhanced chemical vapor deposition (PECVD) method. There are two types of thin film deposition systems in Brno University of Technology.

(1) Parallel plate (capacitive coupling) deposition system and
(2) Helical (capacitive coupling) deposition system.

3.1 The Scanning Probe Microscope

All the scanning probe microscopy experiments discussed in this dissertation were done in a NT-MDT NTegra Prima scanning probe microscope with optical viewing system.

3.1.1 Scanning Probe Microscope basic setup

The NTegra Prima Scanning Probe Microscope comprises the following basic systems:

- Base unit, which supports the completely scanning probe microscope operating system.
- Measuring module, which is made up of measuring head, exchangeable mount, scanner and heating stages, liquid cells etc.
- Protective hood – to protect the scanning probe microscope from external vibration.
- Optical viewing system, and
- Vibration isolation system, which is manufactured by Table stable Ltd., Switzerland under brand name of TS-150. It is a vibration damping system, which is protecting the SPM system from vibration coming through ground.

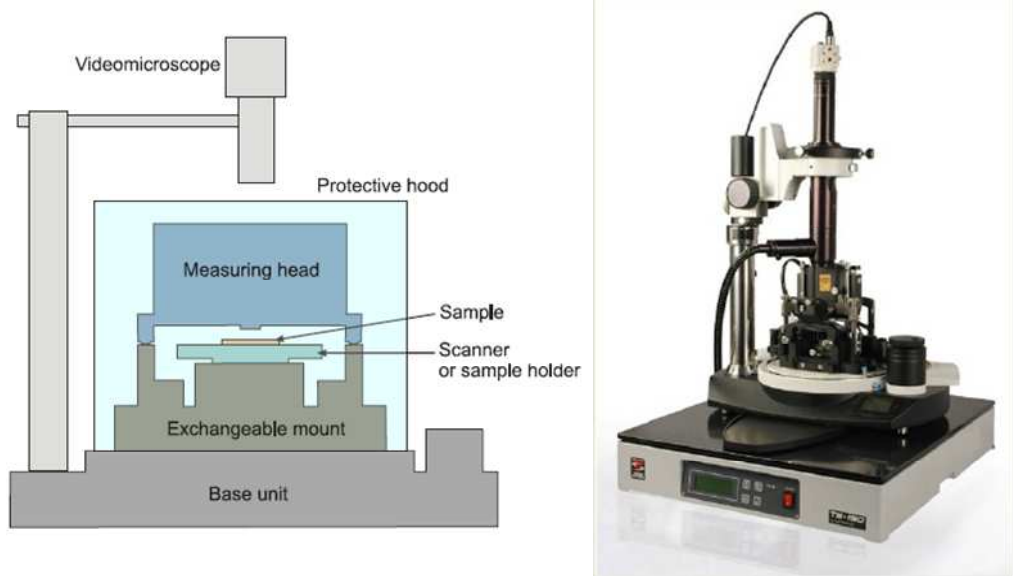

Fig. 3 NT-MDT NTEGRA Prima scanning probe microscope: (a) Schematic illustration of basic modes of the system, (b) photo of SPM system.

The schematic illustration NT-MDT SPM mentioned in Fig. 3. By making changes in measuring modules, it is possible to operate different scanning probe microscopy methods such as Atomic Force Microscopy, Scanning Tunneling Microscopy, Lateral Force Microscopy, Atomic Force Acoustic Microscopy, Electrical Force Microscopy, Lithography etc.

There are many different methods developed under scanning probe microscopy for different purpose. Every method is developing the surface image with the help of some singals. The details about methods, their purposes and useful singals are mentioned in table 1.

SPM Method	Mode	Singal	Purpose	Scan image
AFM	Contact	DFL	Contact topography and surface morphology	Height
	Non contact / semicontact	Mag	Semicontact topography and surface morphology study	Height, Phase, Mag
LF	Contact	DFL	Friction behaviour of surface and tribology characteristics	Height, LF
AFAM*	Contact	Mag	Contact topography and modulus mapping	Height, Mag or Phase
		Phase		
EFM	Non-Contact	Amplitude or phase	Non-contact topography and surface potential	Height, phase or amplitude
KPM	Semicontact mode	Voltage signal	Semicontact topography and surface potential	Height, surface potential

Table 1 Scanning probe microscopy methods

3.2 Nanoindentation Techniques

The nanoindentation experiment was carried out on Triboscope system from Hysitron, Minneapolis, USA. The 2D Triboscope (Hysitron) system attached to an NTegra Prima Scanning Probe Microscope (NM-MDT, Russia) for insitu analysis. The displacement and load resolutions of the Triboscope (Hysitron) instrument are 0.0004 nm and <1 nN, respectively. While, the noise floor for displacement and load are 0.2 nm and 100nN, respectively. The three-plate capacitive force/displacement transducer could be referred as the heart of the testing instrument. It is a pattern technology from Hysitron Company, USA. This transducer provides high sensitivity, large dynamic range, and a linear force or displacement output signal [7]. The maximum load force available from a standard transducer is approximately 10 mN.

Berkovich tip: The Berkovich tip with a radius of curvature of about 150 nm or 50 nm were used for the analysis of thin films, multilayer films and for scratch study. The Berkovich tip with known tip area function is important for correct indentation and scratch experiment. Hence, at proper interval of time, the tip area calibration is carried out.

Sample preparation: For nanoindentation and scratch test, special cyanoacrylate adhesive glue (Loctite 495) is used to stick the sample on steel ring or sapphire plate.

Nanoindentation measurements: Two types of nanoindentation experiments were carried out with this instrument: (a) Conventional nanoindentation test, and (b) Cyclic nanoindentation test.

The drift measurement is very important parameter in indentation test. The drift measurement is performed immediately before the testing. The displacement versus time of linear character was measured at 40 (default) or 120 (suggested) s and the drift rate was evaluated using the linear regression for last 20 (default) or 100 (suggested) s, respectively. The drift rate was used to correct the acquired data from the real indentation testing. The drift rate was maintained in a range of 0.05 nm/s to 0.5 nm/s during indentation experiment.

(a) Conventional Nanoindentation test: Conventional indentation test consist of three segments (1) loading, (2) dwell time or hold time and (3) unloading. Here, the loading segment is followed by a dwell time at maximum load, and followed by an unloading segment. The main variable parameters for conventional test are the different loads (μN) and measurement time (s) of experiment. In general, the loading causes both elastic and plastic deformation under the indenter, while unloading is dominated by recovery of elastic deformation. The upper portion of the unloading curve can be used to calculate the mechanical properties at a given contact depth of the indenter according to the Oliver-Pharr method [5]. A conventional indentation experiment gives only a single value of mechanical properties at a particular load at a time.

(b) Cyclic Nanoindentation test: A new variation of the conventional test is the cyclic nanoindentation test, where the sample is reloaded immediately to higher loads/depths than pervious loading cycle. The important variable parameters in cyclic test are number of cycles, maximum load, displacement exponent, unloading fraction and segments (loading/hold/unloading) time. The multiple load/unload vs. displacement curve is obtained by cyclic indentation experiment. The Oliver-Pharr [5] method is used in a similar way like conventional method to calculate the mechanical parameters from load/unload vs. displacement curve.

Scratch test: The scratch test was used to study the adhesion failures of thin films on silicon substrate. The Berkovich tip with radius of curvature of 150 nm was used for all the scratch testing. For scratch testing, the ramp force scratch positive direction experimental condition was used, The variable parameters in ramp force experiment are the peak force, time of experiment, normal displacement and lateral displacement. The data obtained from scratch experiment critical normal force, critical lateral force and friction coefficient.

4 RESULTS AND DISCUSSIONS

4.1 Single layer film

The AFM and nanoindentation (NI) was used for the analysis of plasma polymer thin films. The various deposition conditions have some effect on the surface morphology and mechanical properties of plasma thin films, which were confirmed by AFM and NI analysis.

4.1.1 Surface analysis by AFM

Thin film preparation: The plasma-polymerized vinyltriethoxysilane (pp-VTES) films were prepared on polished silicon wafers by PECVD using an RF (13.56 MHz) helical coupling plasma [8] system working in the pulse mode. The film deposition was operated at pulsed plasma (t_{on}/t_{off} =1 ms : 9 ms) and 5 W by applying plasma discharge. Single films were deposited during deposition times ranging from 5 to 4800 s, which corresponded to film thickness varying from 13 nm to 8.6 µm.

The pp-TVS films were also prepared on polished silicon wafer by PECVD employing RF (13.56 MHz) working in continuous plasma mode. The set of samples was prepared with the film thickness of about 100 nm at different rf power of 10, 25, 50 and 70 W. The surface morphology of pp-VTES and pp-TVS films were observed by AFM and the RMS roughness was determined from scanned area.

Surface analysis results: The single layer pp-VTES films with thickness ranging from 13 nm to 8.6 µm were prepared at constant deposition conditions. The film thickness increased [9] as the deposition time increased as given in Fig.4. The mean deposition rate was determined from the ratio of the film thickness to deposition time. The mean deposition rate decreased slowly from 250 to 100 nm min^{-1} with the increase in deposition time as shown in Fig. 4. It means that the growth kinetics varied during deposition and dominated the film properties [8].

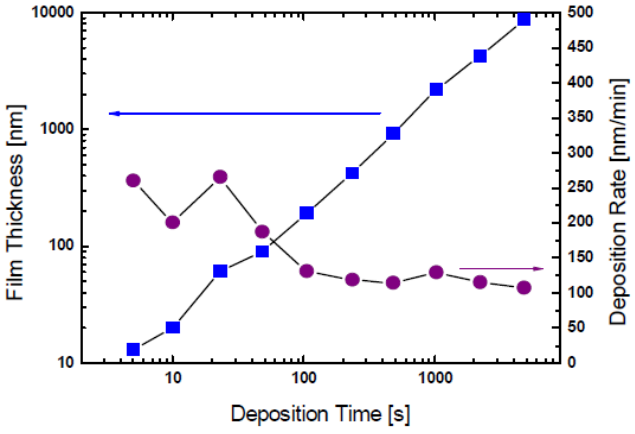

Fig. 4 Film thickness of pp-VTES film and mean deposition rate as a function of deposition time

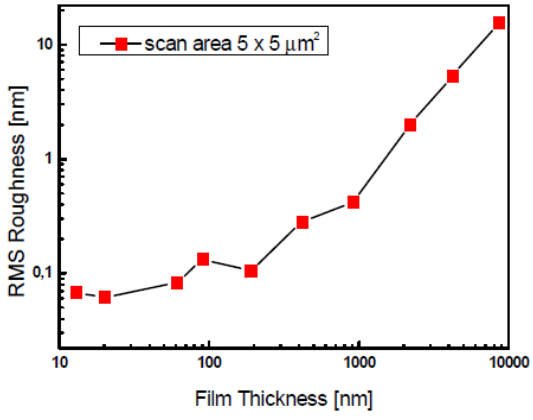

Fig. 5 Evolution of RMS roughness vs. film thickness for pp-VTES films

The information about the surface morphology and the surface roughness for pp-VTES films were obtained from AFM analysis. The scan area 5x5 μm^2 was used for this purpose. The RMS roughness increased from 0.041 nm to 15.46 nm with the increase of film thickness as shown in Fig. 5. The surface morphology of pp-VTES films also changed as film thickness decreases from 8.6 μm to 15 nm. A cauliflower structure on the film surface is apparent for films with thickness ≥ 2 μm.

In another experiment, the RMS roughness of pp-TVS films were increased with increasing RF power, as mentioned in Fig. 6. It could be explained by the slight ablation of the film surface in the glow discharge. It may disrupt the over layer of the material and increase roughness [8].

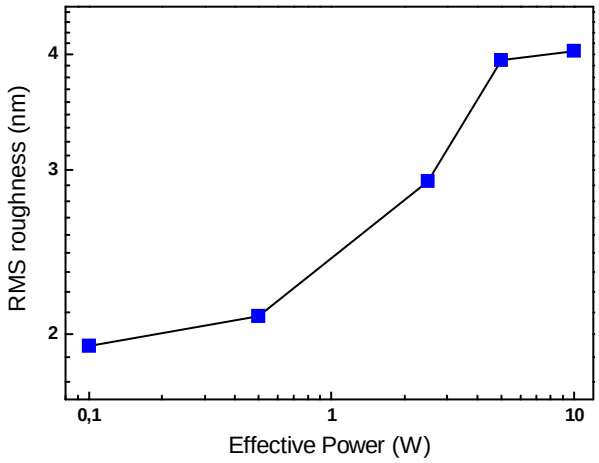

Fig. 6 Comparison of RMS roughness with different RF power used for deposition of pp-TVS films

4.1.2 Mechanical Properties

The mechanical properties of single layer films were determined by nanoindentation using conventional and cyclic indentation technique. The controlled drift correction and proper tip area calibration are important procedure to obtained correct mechanical properties of thin films.

Thin film preparation: Pp-TVS films were prepared by PECVD method by employing RF (13.56 MHz) helical coupling plasma system working in the pulsed mode. The film was deposited silicon wafer, which was pretreated with oxygen plasma (5 sccm, 4 Pa, 25 W) for 10 min. The deposition chamber was cleaned by Ar plasma (10 sccm, 10 Pa) for 10 min to remove remaining oxygen. The pp-TVS film was deposited at a flow rate of 0.50 sccm and a corresponding pressure of 1.3 Pa using TVS plasma under selected effective power. Hence, the pp-TVS films were deposited at different effective power of 0.1, 2.5, and 10 W to influence polymer cross-linking.

The film thickness was measured by spectroscopic ellipsometry and it was 1268 nm (0.1 W), 1035nm (2.5 W), and 960 nm (10 W). All the pp-TVS films were deposited under steady-state plasma conditions, which were monitored by mass spectroscopy. The ellipsometric spectra and their analysis as well as the elemental composition analysis of the films by X-ray photoelectron spectroscopy (XPS) and Rutherford backscattering spectrometry (RBS) confirmed that the deposited films were homogeneous in nature and isotropic materials, with an invariable depth

profile [10]. Therefore, we expect that the mechanical properties of pp-TVS film are also depth-independent.

The mechanical properties measurement of pp-TVS films were carried out at two different experimental conditions (a) drift rate ≤ 0.5 nm/s and (b) drift rate ≤ 0.05 nm/s. The main purpose of these experiments is to check the influence of different drift rate on mechanical properties measurement of pp-TVS film.

Set 1 (drift rate ≤ 0.5 nm/s): The mechanical properties of pp-TVS film deposited at 10 W were evaluated in set 1 experiment. A Berkovich tip with a radius of curvature of about 150 nm was used. The drift rate was measured for 40 s and evaluated from the last 20 s. The drift rate was ≤ 0.5 nm/s. In set 1 experiment [11], we found out that the dwell time and loading/unloading times >5 s produced a progressive increase of the tip displacement likely due to a high system drift (<0.5 nm/s) not being correctly subtracted at prolonged measuring times. The increased tip displacement at prolonged measuring times resulted in underestimation of the Young's modulus and hardness. Thus, the cyclic nanoindentation using only 7 cycles during 90 s (measuring time) gave unsatisfying results.

Set 2 (drift rate ≤ 0.05 nm/s): The mechanical properties of pp-TVS films deposited at 0.1, 2.5 and 10 W were evaluated. A Berkovich diamond indenter with a radius of curvature of 50 nm was used. The drift rate was measured for 120 s and evaluated from the last 100 s. Hence, the drift rate was ≤ 0.05 nm/s for all the measurements.

Two types of nanoindentation test were done:

(i) Conventional indentation experiment was carried out for pp-TVS films to obtain the depth profile of mechanical constants until 15-20% of the film thickness. The loading, unloading, and dwell time was kept constant at 5 s for all the measurements.

(ii) Cyclic indentation experiment was also carried out to obtain the depth profile of mechanical constants until 15-20% of the film thickness but applying many loading cycles in one single indentation, while the unloading fraction was kept constant at 0.8.

Results: In this study, we reduced the system drift significantly (≤0.05 nm/s) due to prolonged (3 min) contact of the indenter with the sample surface before nanoindentation measurement. The longer the probe is on the sample surface the lower the drift will be [12]. Typical values of drift rate were ranging from 0.01 to 0.05 nm/min for both the conventional depth-sensing and cyclic nanoindentation methods.

First, the pp-TVS films deposited at an RF power of 0.1, 2.5, and 10 W were analyzed by conventional depth sensing technique. The 20 single indentations were performed on all the films at different loads to study the depth profile of mechanical properties until 15-20% of the film thickness. The Oliver-Pharr method [5] was used to evaluate mechanical properties. The indentations into increasing indenter displacement enabled us to construct dependences of the

Young's modulus and hardness on the contact depth (vertical distance along which contact is made).

Next, all the pp-TVS films were analyzed by cyclic nanoindentation method under similar experimental conditions like the conventional method, i.e., loading/unloading and dwell time of 5 s. The cyclic nanoindentation experiment consisted of 20 loading-partially unloading cycles with unloading fraction of 0.8 and the loading increased using displacement exponent of 2 (exponential function). The single indentation consisting of 20 cycles lasted for 300 s. The Oliver-Pharr method was used to evaluate the mechanical parameters from all the unloading segments at the corresponding contact depth. The Young's modulus and hardness as a function of the contact depth are compared in Fig. 7 for both the methods - conventional (full symbol) and cyclic (empty symbol) nanoindentation. Only two examples are presented corresponding to the pp-TVS film deposited at lower (0.1 W, Fig. 7 a) and higher (10 W, Fig. 7 b) power as character of plotted dependences is the same for the film deposited at 2.5 W. It can be seen that both the methods gave very similar results in case of a softer (0.1 W) and a stiffer (10 W) film as well except for region of small contact depth (5-30 nm); the discrepancy is discussed in later text. Thus, a reduced system drift enabled us to not only obtain more precise data and similar results for both the methods but also accelerate depth analysis of mechanical properties using cyclic nanoindentation.

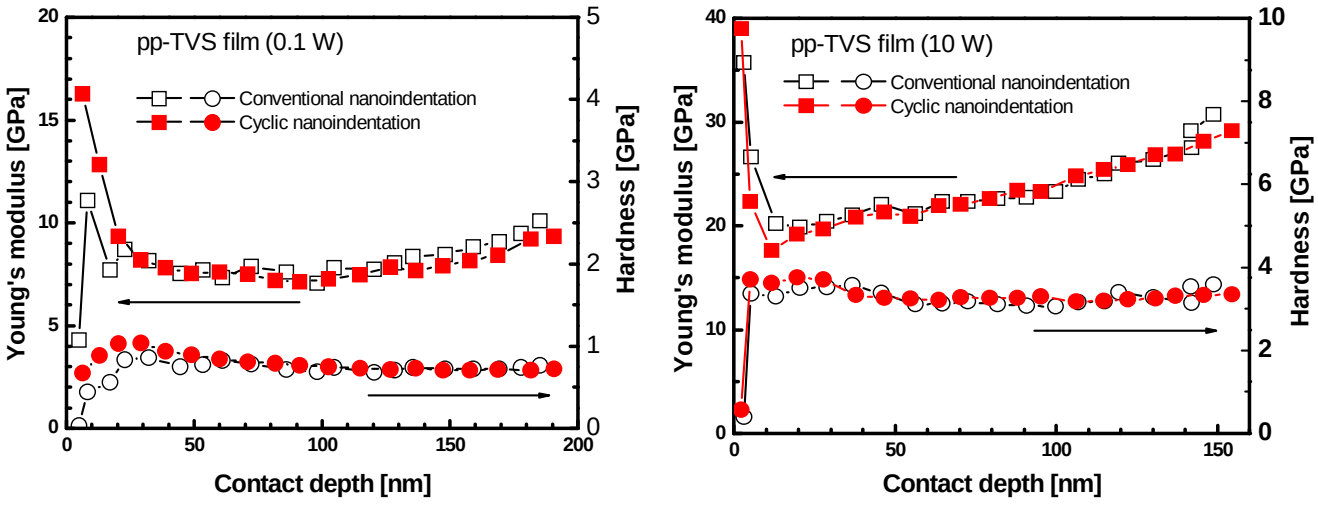

(a) (b)

Fig. 7 Comparison of Young's modulus and hardness vs. contact depth using conventional (empty symbol) and cyclic (full symbol) nanoindentation for pp-TVS films deposited at (a) 0.1 W, (b) 10 W.

Furthermore, the cyclic indentation method was used to study the depth profile of mechanical properties for pp-TVS films deposited at different powers in more details. Five cyclic nanoindentation experiments, each for 20 cycles, were used for each sample to estimate reproducibility of measurements. Therefore, the mean value and standard deviation were determined for the Young's modulus, *E*, and hardness, *H*, as given in Fig. 8 for all the films. The

modulus increased abruptly accompanied by higher standard deviation decreasing the contact depth in range 5-30 nm from the film surface and this phenomenon will be discussed in next paragraph. The Young's modulus was reproducible and increased gradually for higher contact depth due to an influence of stiffer substrate (silicon wafer: E = 170 GPa, H = 11 GPa). Extrapolation (red dashed line) of the bottom portion of modulus curve (low standard deviation) to zero contact depth should result in a value of the Young's modulus for the pp-TVS film only (without substrate influence) [13]. The extrapolated values are given in Table 2. The trend of the hardness characteristics is similar for all the films and the hardness is approximately constant for higher contact depth used to evaluate (red dashed line) the mean value (Table 2). The contact depth (vertical blue dotted line) corresponding to the 10% rule is marked in Fig. 8 and the corresponding values of Young's modulus and hardness are given in Table 2. There is no difference in hardness data due to the horizontal character of hardness plot. However, an increasing difference between the extrapolated and 10%-rule values can be found for the Young's modulus with enhanced film stiffness and a difference of 29% due to the substrate influence was determined for the film deposited at a power of 10 W. It means that there is no so-called "flat region" for stiffer films, where the substrate influence is negligible, and an application of 10% rule results in wrong data. It is clearly seen from Table 2 that the enhanced power resulted in higher mechanical properties of deposited film. The increase of mechanical properties could be related to a higher cross-linking and/or an alteration of chemical structure with increasing organic character of plasma polymer, when the effective power was enhanced [14].

RF power [W]	Extrapolation		10% rule		Difference	
	E [GPa]	H [GPa]	E [GPa]	H [GPa]	ΔE [%]	ΔH [%]
0.1	7.9	0.69	8.2	0.69	4	0
2.5	14	2.0	15	2.0	7	0
10	17	3.0	22	3.0	29	0

Table 2 Mechanical properties of pp-TVS films determined by extrapolation to zero contact depth, using the 10% rule, and their differences.

The mechanical properties of thin films can be measured at a shallow depth, i.e., near to the thin film surface, if several conditions are fulfilled [15]: (i) sharp indenter, (ii) careful calibration of the indenter area function, (iii) minimal system drift and using drift correction, (iv) smooth sample [16]. Our measurements fulfill the conditions; the area function was calibrated for indenter displacement starting from 5 nm and the RMS roughness of films varied with power from 2.0 nm (0.1 W) to 5.8 nm (10 W) as measured in scanning area 5 μm × 5 μm by AFM. Moreover, the mechanical parameters could be influenced by the pile-up phenomenon, [17]. However, for pp-TVS films pile-up was not confirmed by AFM observations. Despite favorable condition for nanoindentation measurements, an increase of the Young's modulus with

diminished contact depth in surface region 5-30 nm can be found in Fig. 8 accompanied by increased standard deviation marked by the error bar. Detailed analysis of unloading curves revealed increasing noise of measured data close to the film surface, especially for softer film due to a low contact stiffness at low indenter-film contact area resulting in non-reproducible modulus data and thus increasing standard deviation (error bar). Therefore, the modulus data are incorrect in surface region up to ~30 nm (0.1 W), 20 nm (2.5 W), and 10 nm (10 W) with respect to the stiffness of pp-TVS film. The hardness data seemed to be more reproducible in the surface region.

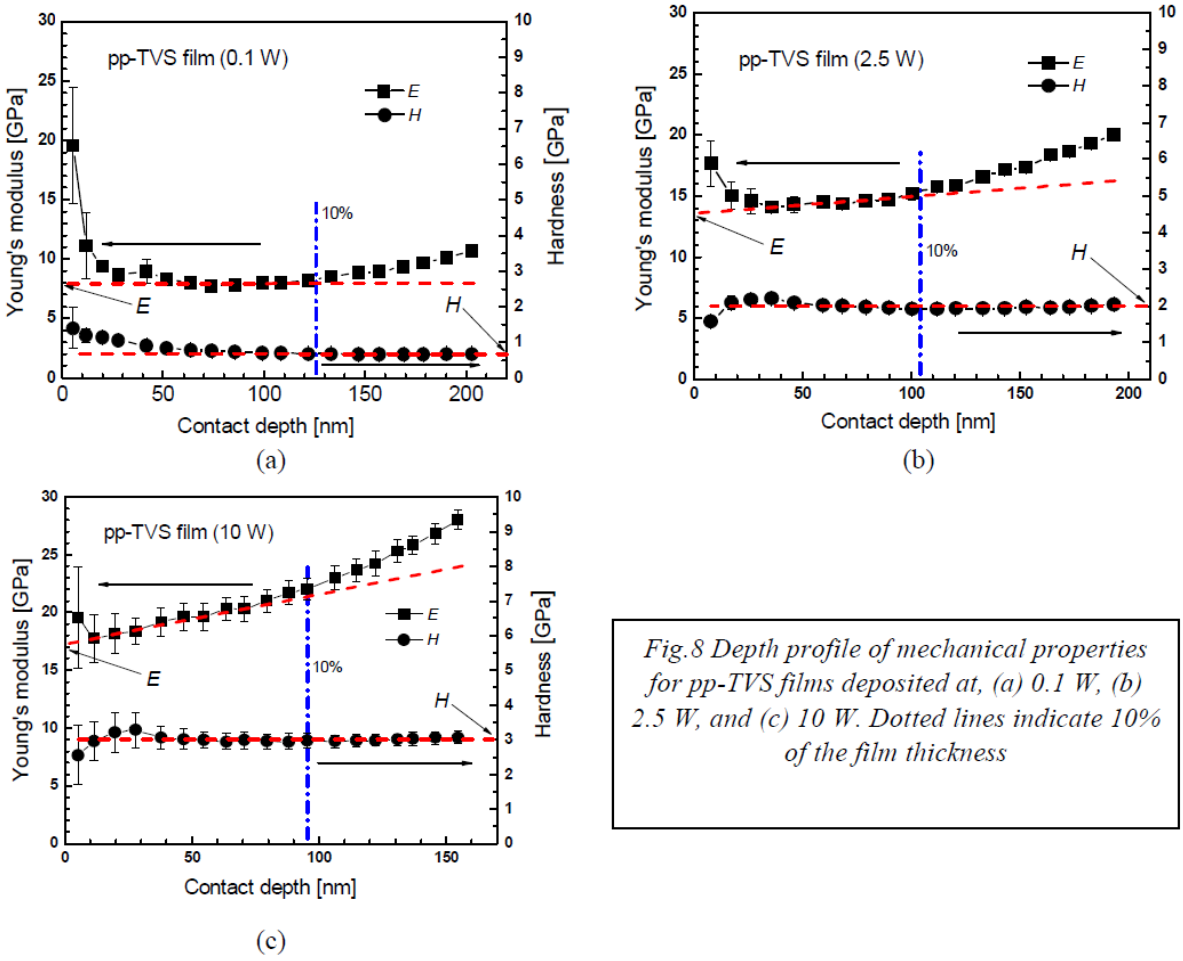

Fig.8 Depth profile of mechanical properties for pp-TVS films deposited at, (a) 0.1 W, (b) 2.5 W, and (c) 10 W. Dotted lines indicate 10% of the film thickness

4.2 Hybrid film

Thin films in a form of hydrogenated amorphous carbon-silicon (a-SiC:H) alloy were deposited on polished silicon wafers (100) from tetravinylsilane monomer using PECVD (13.56 MHz). The surface morphology and mechanical properties of the films were analyzed by AFM, nanoindentation, finite element analysis (FEA) simulation and AFAM techniques.

Thin film preparation: Plasma polymer films of tetravinylsilane monomer (TVS) were deposited on polished silicon wafers by PECVD employing an RF (13.56 MHz) capacitive coupling system

with plan-parallel electrodes [18]. The vacuum system was evacuated to a basic pressure of 1 x 10^{-5} Pa. The substrates were pretreated with argon plasma (10 sccm, 5 Pa, 5 W, continual mode) for 10 min to improve the film adhesion. The plasma polymerized tetravinylsilane (pp-TVS) films were deposited at a mass flow rate of 3.7 sccm and the effective power was in a range of 10 – 70 W. The deposition rate was ranging from 140-173 nm/min as a function of the deposition conditions. Uniform plasma polymer films were deposited at a film thickness of about 1 µm.

4.2.1 Surface morphology analysis by atomic force microscopy

The surface morphology of all pp-TVS films were studied by semi-contact AFM. The RMS roughness value of pp-TVS films were obtained from the surface morphology analysis. The grain structure of all the films was extensively investigated by image analysis with the help of Nova software (NT-MDT, Russia). It helped to produce the histogram of grain size distribution for pp-TVS films. The mean grain size value for particular pp-TVS film was obtained from it. The obtained RMS roughness and avg. grain size for each pp-TVS films mentioned in table 7.

In surface morphology analysis, it was observed that the grain size were increased from 29 nm to 500 nm (table 7) for pp-TVS films as the deposition conditions changed from 10 to 50 W. The large number of bigger grains was observed for pp-TVS film (50 W). The big grains were distributed through the film and hence the RMS roughness of the film was 8.5 nm. When the surface morphology of plane area (area between the large grains) was characterized, the average RMS roughness of it was only 0.57 nm. The average grain size distribution for this film was increased to 500 nm because of large number of big grains.
In case of pp-TVS film (70 W), the big grains were found in huge numbers and they started to agglomerate i.e. fused in each other. The average grain size and RMS roughness of this film was 241 nm and 21.7 nm, respectively. The average grain size for this film was lower than the film (50 W) because of application of higher threshold value for film analysis. The main reason behind higher threshold value was the agglomerates nature of big grains. The average RMS roughness of plane area (area between the big grains) was only 0.4 nm. The intensity of smaller grains was decreased ever further compare to pp-TVS film (50 W).

In simple words, the surface morphology i.e. surface roughness was increased from 3.4 nm to 21.7 nm for pp-TVS films as the deposition conditions changed from 10 to 70 W (table 7). The grains height and size distribution was also increased with RF-power. The surface morphology observed in AFM analysis for pp-TVS film (70 W) could be explained by Messier model [19] proposed for silicon film, mentioned in Fig. 9. According to it, the grains and the plane area were grown together as a crystal structure from the point of nucleation.

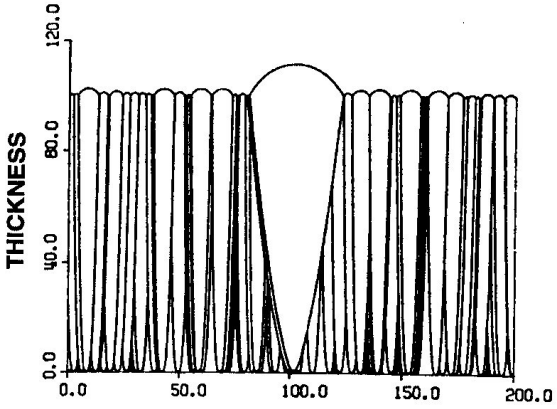

Fig. 9 The cone growth model by Messier [19]

4.2.2 Mechanical Properties

The mechanical properties of pp-TVS films were characterized by nanoindentation method in the plane area of the film, i.e., the area between the grains for comparison purpose. The mechanical properties were studied out at the 10 % of film thickness to avoid the substrate effect. At least five nanoindentation experiments were used estimate the reproducibility of the measurements. Therefore, the mean value of the Young's modulus, *E*, and hardness, *H*, were given in the Table 3. It is clearly seen from the Table 3 that the enhanced power resulted in higher mechanical properties. The increase of mechanical properties could be related to a higher cross-linking and/or alteration of chemical structure with increasing organic character of plasma polymer [14].

RF power [W]	Surface analysis		Mechanical Properties		
	Avg. RMS roughness [nm]	Avg. grain size [nm]	Contact depth [nm]	*E* [GPa]	*H* [GPa]
10	3.4	29	99.6	11.8	0.84
20	3.7	48	97.5	24.4	2.88
25	4.0	52	112.7	32.7	4.62
50	8.5	500	96.7	63.0	7.40
70	21.7	241	92.1	81.4	8.84

Table 3 Mechanical properties of pp-TVS films

RF power [W]	Position	Young's modulus		Hardness	
		E [GPa]	Std. Dev	*H* [GPa]	Std. Dev
25	Plane	32.7	0.7	4.62	0.14
	Grain	27.8	1.1	3.44	0.26
50	Plane	63.0	1.8	7.40	0.19
	Grain	35.7	3.1	3.21	0.23
70	Plane	81.4	0.7	8.84	0.13
	Grain	41.8	3.8	3.48	0.67

Table 4 Detailed mechanical properties of plane and grain of pp-TVS film deposited at 25, 50 and 70 W

Further, the detailed analysis of mechanical properties of plane area as well as big grains in all pp-TVS films were carried out. The obtained mechanical properties such as the Young's modulus, *E*, and hardness, *H*, for plane area as well as central area of grains for selected pp-TVS films (25, 50 and 70 W) are mentioned in Table 4. There is difference in mechanical constants for plane area and grains. It is observed from the Table 4 that the enhanced power resulted in higher differences in mechanical properties of plane and grain. For the pp-TVS film (70 W), the difference in mechanical properties is almost 50 %. This data leads to a possibility of hybrid nature of pp-TVS film being deposited at higher RF power.

As mentioned previously, the nanoindentation data indicates the possibility of two different kind of material with different mechanical properties to be present in pp-TVS film deposited at higher RF-power. The difference in measured data of plane area and grains can be explained by two possibilities:

(1) Effect of different geometry, i.e., different geometry of plane area and grains may lead to different deformations under indentation load,

(2) Difference in mechanical properties of plane area and grains.

To check the 1st possibility, the depth profile of mechanical properties was analyzed for pp-TVS film (70 W). The selected big grains were used whose height were around 120 nm. The obtained data such as the Young's modulus vs. contact depth and hardness vs. contact depth are mentioned in Fig. 10 (using -□- symbol for plane area and -○- symbol for grain). The linear extrapolation was used to obtain the true Young's modulus and hardness for plane area of pp-TVS (70 W) film, which were found out to be 73 GPa and 8.7 GPa respectively. The values of Young's modulus and hardness obtained by linear extrapolation were little lower than the value obtained by 10 % rule (mentioned in Table 4). The influence of hard silicon substrate on mechanical properties was clearly seen around 10 % of the film thickness i.e. around 100 nm of the film thickness. The data obtained from the depth profile study were sent for finite elemental analysis.

For better understanding, the simulated data (red line) were compared with depth profile data (black point) mentioned in Fig.10. It is clearly seen that the mechanical properties (Young's modulus, hardness) obtained for the plane area from both methods (nanoindentation and simulation) were having the same trend and harmony. In a similar fashion, the hardness data obtained from both methods for grains were having the same trend and within the error margin. However, the Young's modulus of grain was showing some difference. This difference helped to understand that at some extent there is a possibility of effect of different geometry of plane area and grain on nanoindentation data because of their different deformation under the loading conditions.

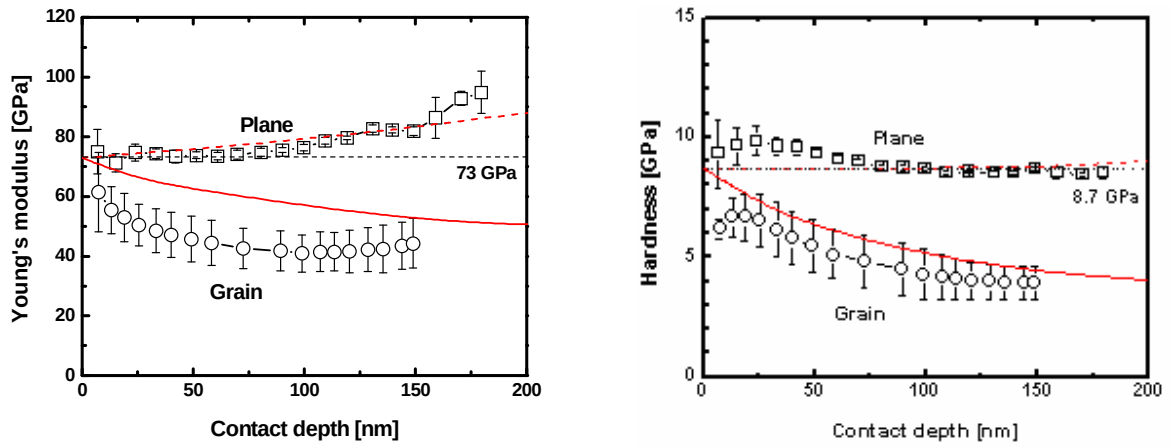

Fig. 10 Comparison of FEA simulated data with nanoindentation data for pp-TVS film [70 W]

4.2.3 Surface analysis by Atomic Force Acoustic Microscopy

The AFAM experiment was carried out on pp-TVS film deposited at 70 W RF power. It was used to measure the magnitude change of cantilever vibrating near to its resonance frequency. The obtained data were mentioned in Fig. 11. The topography (Fig 11 a) is a contact mode topography produced simultaneously with mag AFAM image. In mag AFAM image (Fig 11 b); the dark part of the scale represents the material, which is softer in nature. On the contrast, the bright part of the scale represents the stiffer material. So it was concluded from the AFAM image that the grains were softer in nature compared to the plane area i.e. the grains were having the lower mechanical properties than the plane area. This result indicated the possibility of nanocomposite nature of this film.

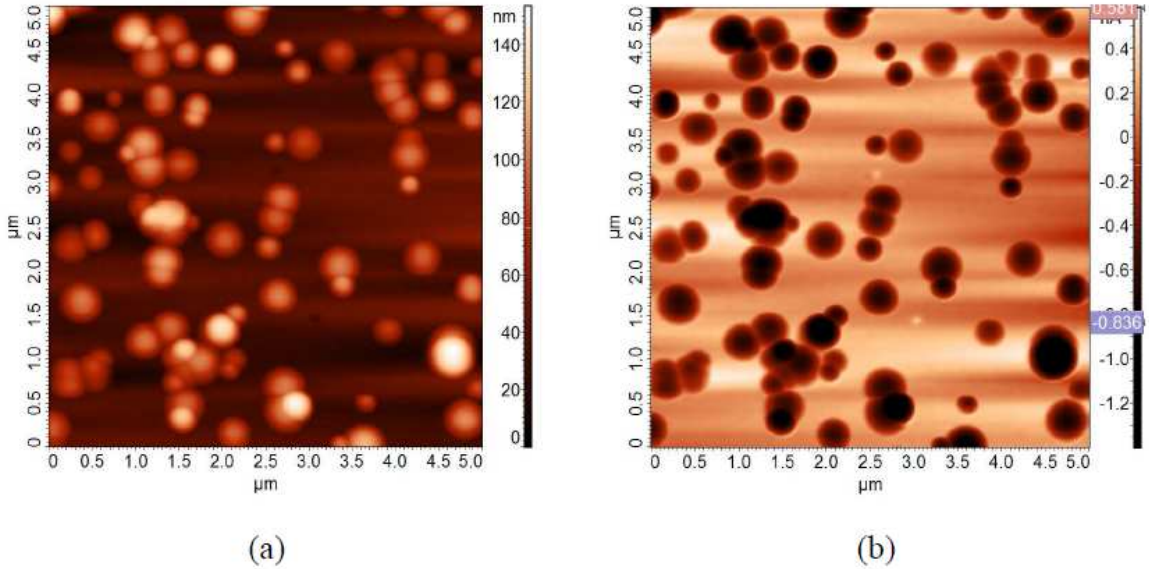

Fig. 11 Images of the surface of pp-TVS film deposited at 70 [W]: (a) topography map; (b) AFAM mag contrast

4.3 Adhesion test

The adhesion test for series of samples were carried out by nanoscratch test with the help of Hysitron triboscope instrument. The nanoscratch tests were performed with a Berkovich diamond indenter of 150 nm tip radius curvature. There were four experiments carried out to study the adhesion failurity of plasma-polymerised thin films on silicon substrate.

Thin film deposition: Plasma-polymerised tetravinylsilane (pp-TVS) films were deposited on polished silicon wafers by PECVD empolying an RF (13.56 MHz) working in continuous plasma mode. The vaccum system was evacuated to a basic pressure of 1 x 10^{-5} Pa. The substrates were pretreated with argon plasma (10 sccm, 5.0 Pa, 5 W) for 10 min. The mass flow rate of TVS monomer is 3.8 sccm. Pp-TVS samples were prepared in 3 sets for adhesion failurity experiment:

(i) There are three samples A, B and C prepared at same deposition conditions of 10 W and similar in film thickness of 100 nm. These samples were used for checking the reproducibility of adhesion behaviour and for influence of sample aging. While, the sample A was used for scratch experiments with different scratch speed.

(ii) A set of samples was prepared at the same 10 W power but difference in film thickness (25, 54, 99, 197, 334 and 468 nm) by varying their deposition time. These samples were used to study the effect of different film thickness on adhesion failurity.

(iii) Another set of samples were prepared with the similar film thickness of about 100 nm but at different RF power of 10, 25, 50 and 70 W. Due to differece in deposition condition, these films were having different mechanical properties. Further, scratch tests were carried out to correlate the effect of different mechanical properties of thin films and their scratch behaviour.

4.3.1 Study of effect of different scratch speed on measured data

This experiment was carried out on sample deposited at 10 W and having the thickness of 99 nm. By varying the scratch time from 120 to 7 s, the loading rate was also changed from 16.7 µN/s to 285.7 µN/s. Hence, the scratch speed was also changing from slowest to fastest. The data were summarized in Fig 12. It was observed from the Fig. 12 that the critical normal force was slightly higher for increased scratch speed due to stress. The fracture occurs at higher or lower of the scratch speed of about 100 (µN/s) were considered consistent and it was overlapping in the range of measurement error (see in Fig. 12).

The increase in strength at the higher speed could be explained by the reason that the material would have got less time to response or deform, hence the measured critical power was higher than that would have been at a lower speed. The present experiment indicated that the changing in scratch speed has a little effect on obtained adhesion failure data. Hence, now on words the selected scratch time used for further experiments was 30 seconds with a length of 10 µm corresponding to a scratch speed of 66.7 µN/s.

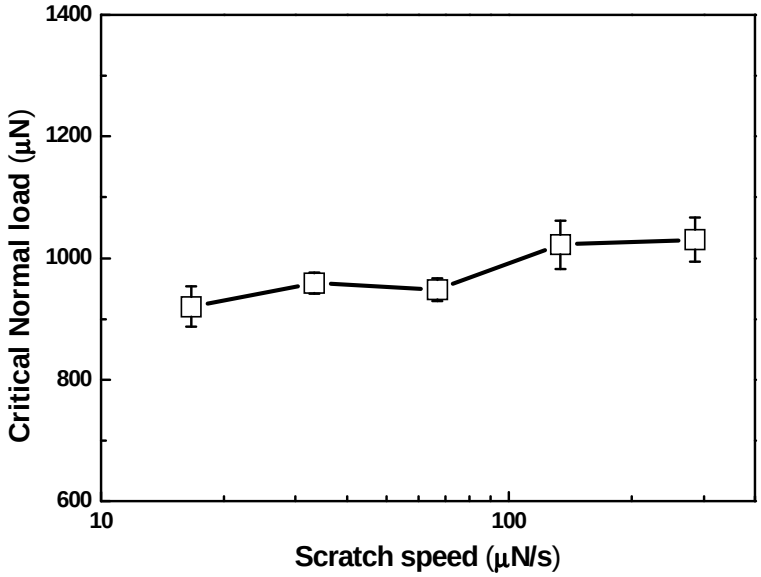

Fig. 12 Critical normal load (μN) vs. scratch speed (μN/s) for pp-TVS film deposited at 10 W

4.3.2 Reproducibility of the adhesion data

The samples used for this experiment were prepared at 10 W, having the same mechanical properties (Young's modulus of 12 GPa, Hardness of 0.8 GPa) and about 100 nm in thickness. The samples A, B and C were prepared at different time interval of 06/2008, 10/2009 and 11/2009, respectively. The aim of the expeiment was to evaluate the reliability of the plasma deposition of reproducible thin layers and to reveal a possible aging effect. 10 sets of exepriments were carried out for each sample to produce the average value of critical normal force with std. dev, mentioned in Table 5. The mean critical normal force of these three samples is approximately 884. The mean value obtained from the experiments do not exceed the acceptable range of measurement errors of 10 %. The obtained data indicate that the plasma deposition equipment is capable to reproduce the organosilicon thin films with similar adhesion characteristics.

Samples	Average Critical Normal Force (μN)	Std. Dev. (μN)
A	811	44
B	948	19
C	893	41

Table 5 Scratch data of sample A, B and C prepared at different time interval

4.3.3 Effect of different film thickness on adhesion failures

As mentioned previously in film preparation, a series of pp-TVS films deposited at 10 W rf-power discharge with variable film thickness of 25, 54, 99, 197, 334 and 468 nm were used for this experiment. Ten scratch experiments were used for each sample to estimate reproducibility of measurements. The scratch behaviour of each sample were scanned in height mode and mag mode image by the help of AFM.

The scratch experimental data such as the critical normal load and critical lateral load with std. dev. mentioned in Table 6 for different film thickness. It is clearly seen from Table 6 that enhanced film thickness from 25 nm to 468 nm resulted in higher critical normal load from 212 µN to 8864 µN and higher critical lateral load from29 µN to 2049 µN for adhesion failurity. The critical normal load increases approximately linearly with film thickness upto a thickness of 334 nm. In general, if we assume that the adhesion is the same and critical load is determined by the extent of the deformation, an increased film thickness requires an increased indenting load to obtain the same deformation so that the critical normal load increases with the film thickness [20].

Film thickness (nm)	Critical Normal load (µN)	Std. Dev.	Critical Lateral load (µN)	Std. Dev.
25	212	17	29	3
54	414	25	71	3
99	893	41	206	10
197	2181	122	455	24
334	3936	117	849	49
468	8864	650	2049	184

Table 6 Influence of different film thickness of pp-TVS films on scratch data

The correalation of scanned AFM images with scratch measurement data was really helpful to understand the mechanism of adhesion failurity of pp-TVS films as thickness increased from 25 nm to 468 nm. The pp-TVS film of 25 nm was deformed under the normal critical load of 212 µN and normal lateral load of 29 µN, mentioned in Table 6. It was observed from AFM images that it is really difficult to see the delamination point for pp-film becuae of elastic recovery. Only a small amout of deformation was observed. Simlar kind of problem was observed for the scratch data of this film mentioned in Fig. 13. For this film, there was no disturbance in normal force vs. lateral force plot observed. But a small transition repetative in normal force and lateral force was seen. As the film thickness was increased from 54 nm to 468 nm, the delamination point of each film was clearly observed from normal force vs. lateral force plots.

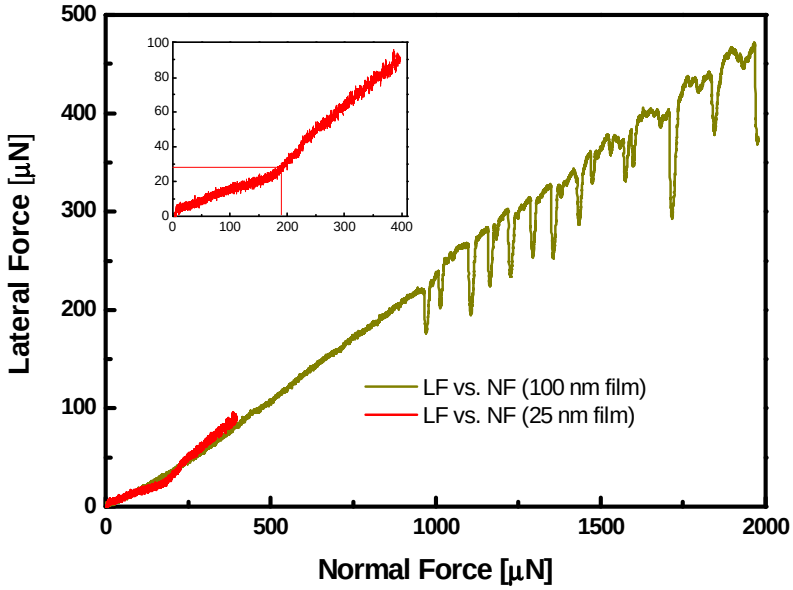

Fig. 13 Comparison of Lateal force (µN) vs. normal force (µN) data of pp-TVS films having thickness of 25 nm and 100 nm

In comparison with the film of 25 nm, the pp-TVS film of 468 nm showed a clear delamination point on scratch track. It showed a large area of the film around the second half of the scratches were completely delaminated. The large part of the film was delaminated and removed it might be due to the higher internal stress in the film caused by higher normal force. Thus, one can conclude that the thicker film has better adhesion to the substrate.

One interesting point came in focus when the lateral foce vs. normal force plot was observed carefully for the pp-TVS film of thickness 468 nm, stated as Fig. 14. It is seen from Fig. 58 that there is a possibility of two normal critical force ($N_{C1,}$ N_{C2}) and two lateral critcal force (L_{C1}, L_{C2}) for this film. The 1st point (N_{C1}, L_{C1}) was observed with a very small changes on scratch track and plot. While, the 2nd point was clearly visible and hence it was used as the data in current study.

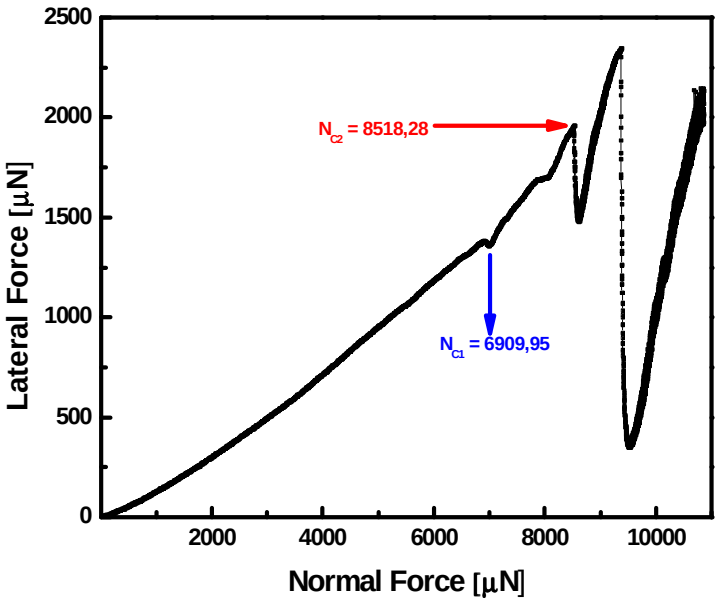

Fig. 14 Lateal force vs. normal force plot for pp-TVS film of 468 nm

Similar kind of behavior also observed for the pp-TVS film of 334 nm thickness. On the basis of the scratch test and the scanned AFM images conclude that the film thickness has a significant impact on the adhesion failurity data.

4.3.4 Effect of different mechanical properties of thin films on adhesion behavior

A series of films were prapared at different rf power of 10, 25, 50 and 70 W with similar film thickness of about 100 nm for comparing the scratch adhesion data. The enhanced RF power resulted in higher mechancial properties of deposited film i.e. the pp-TVS films of 10, 25, 50 and 70 W were having the Young's modulus of 12, 33, 63 and 81 GPa, respectively and hardness of 0.8, 4.6, 7.4 and 8.8 GPa, respectively. The increase of mechanical properties could be related to higher cross-linking of plasma polymer, when the effecitve power was enahnced [14]. The scratch experiment were performed on each sample for 10 times to obtain the mean value and standard deviation of critical normal load and critical lateral load, as given in Table 7.

Deposition conditions (W)	Critical normal load (μN)	Std. Dev.	Critical Lateral Load (μN)	Std. Dev.
10	893	41	206	10
25	1473	129	280	35
50	7456	1147	1649	257
70	2396	235	527	57

Table 7 Scratch data such as the critical normal force and critical lateral force of pp-TVS films deposited at different RF-power

It is clearly visible from Table 7 that the increased RF power from 10 to 50 W resulted in higher critical normal load and higher critical lateral load. Hence, the better adhesion at higher RF power can be explained by the enhancement of cross-linking nature of the films. The pp-TVS film deposited at 70 W was having the lower scratch data compared to the film deposited at 50 W, despite this film has better mechanical constants than 50 W film. This behavior lead to an explanation that this film was having the strong network in the film but week linkage between the film and substrate. This behavior could be explained by more internal stress in the film.

The AFM scratch images helped to study the visible point of adhesion failure on thin films i.e. the place where the tip broke the path of the scratch in the thin films to touch the substrate. The initial phase of scratches was not seen clearly due to a very small amount of force and elastic recovery. Further, the middle section of scratches was clearly visible due to higher amount of deformation taking place at high forces. The scratches were more clearly visible in softer films compared to the stiffer films.

4.4 Multilayer film

A novel way was used to intensively characterize the multilayer structure of the film by scanning probe microscopy and nanoindentation method. For that purpose, single layer and multilayer tetravinylsilane films were deposited by PECVD method.

The single layer tetravinylsilane film (A) of thickness 1217 nm was prepared at an RF-power of 10 W. The film (B) of thickness 748 nm was deposited at an RF-power of 0.1 W. The multilayered a-SiC:H film consisted of 10 individual layers of film – A and film – B type with a buffer layer in the bottom. The total thickness of multilayer film was around 2 µm. In which, the buffer layer was having thickness of 1 µm and the thickness of individual layers of multilayer film was around 100 nm, which was measured by using spectroscopic ellipsometry (SE).

4.4.1 Surface analysis of thin films in normal direction

The surface morphology of single layers (A & B) and the multilayer film had studied out by the help of semi-contact mode AFM technique. The root mean square (RMS) roughness was calculated from the surface morphology. The RMS roughness of individual films A and B was 2.4 nm and 1.4 nm, respectively. While, the RMS roughness of multilayer a-SiC:H film was 4.0 nm. The multilayer film was having such a high roughness because of the contribution of roughness of individual layers in it.

The mechanical properties such as the hardness and the Young's modulus of single layer film A and film B have been studied out by nanoindentation are mentioned in Table 8. The mechanical properties were measured until 10 % of the film thickness to avoid the influence of substrate in measurement. The standard deviation values were within the error bar (10 %); hence, they were not mentioned here.

Individual film	Deposition conditions (w)	Film thickness (nm)	Contact Depth (nm)	Mechanical properties	
				Young's Modulus (GPa)	Hardness (GPa)
A	10	1217	106.3	22.1	2.72
			30.2	15.4	1.69
B	0.1	748	65.8	9.78	1.08
			47	9.63	0.94

Table 8 Mechanical properties of Single layer films

Further, the nanoindentation method was used to study the depth profile of mechanical properties for multilayer a-SiC:H film in normal direction (i.e. direction perpendicular to the surface). The Young's modulus and hardness as a function of the contact depth are mentioned in Fig 15. Here, the influence of bottom layers and the substrate in measurement of mechanical properties can be observed from the progressive increased of the curves. Hence, the mechanical constant of the individual layers cannot be determined by nanoindentation measurements in normal direction to the surface of multilayered film.

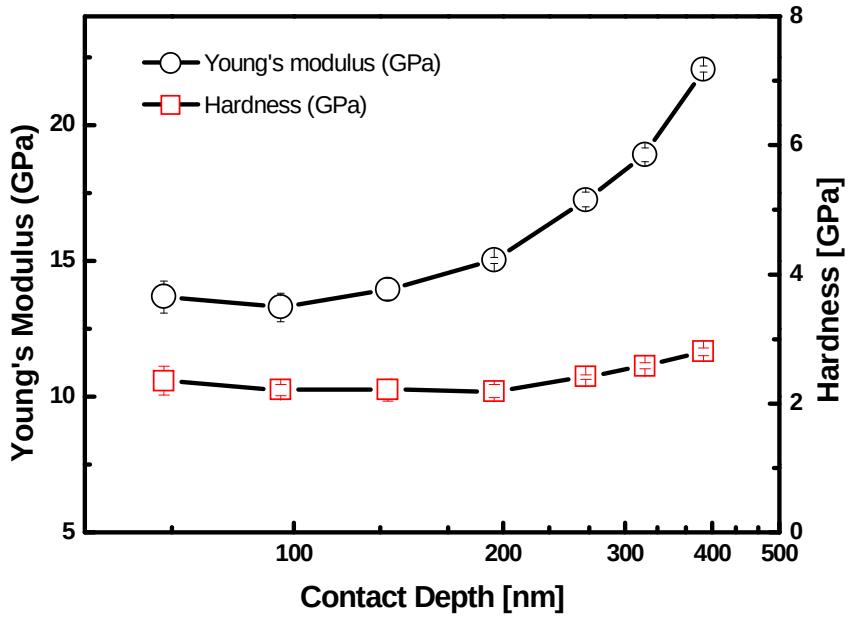

Fig. 15 Young's modulus and Hardness vs. Contact Depth for a-SiC:H multilayer film in normal direction.

4.4.2 Multilayer film analysis by Atomic Force Microscopy and nanoindentation

Normally, the multilayer structure of thin films was observed with the help of transmission electron microscopy (TEM) or high-resolution transition electron microscopy (HRTEM) after making the cross section of that particular film by the help of ultramicrotomy or ion beam thinning method [21]. As well as, the mechanical properties of multilayer films were evaluated by many researchers in normal direction only as it was mentioned in Fig 15. However, in our present study, a novel approach was used to characterize the structure, morphology and mechanical properties of individual layers in the multilayer a-SiC:H system by sectioning method. The 10-layered a-SiC:H film was sectioned at a small angle of 4° by a Leica EM UC6 ultramicrotome as mentioned in Fig 16. The 1-µm-thick buffer layer was used to protect the diamond knife from damage during sectioning process.

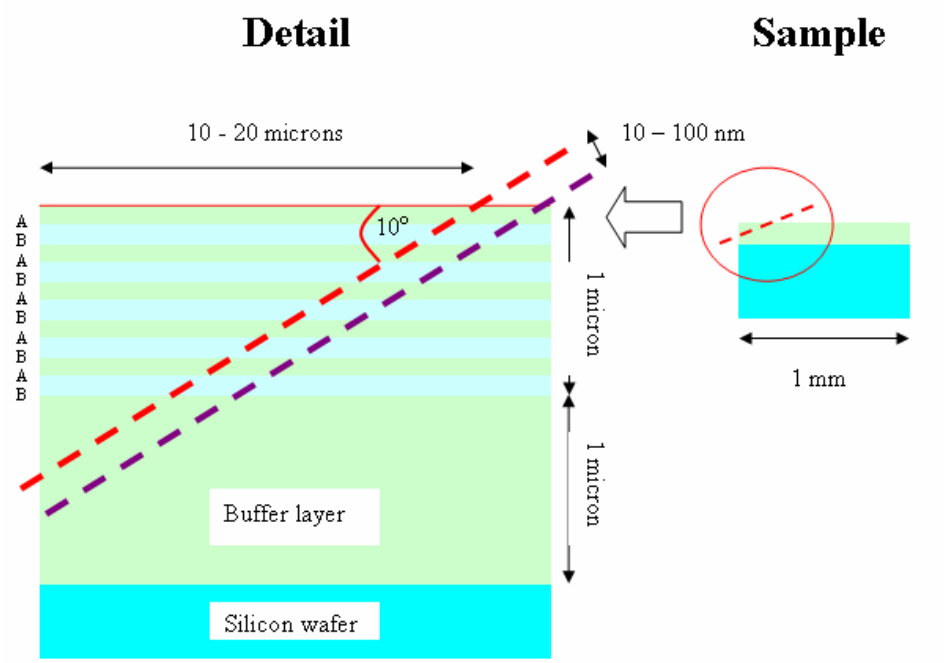

Fig. 16 Schematic diagram of sectioning of multilayer film.

After sectioning, the individual layers of multilayer film were analyzed in details by AFM, nanoindentation, Lateral Force Microscopy and Atomic Force Acoustic Microscopy.

First, the surface morphology of uncovered multilayered a-SiC:H film was examined by non-contact mode AFM. This enabled us to recognize the individual layers as mentioned in Fig 17. It can be seen from Fig. 17 (a) that the non-contact mode topography of eight individual layers, which mentioned from right to the left with the topmost layer at the extreme right side corner. The magnitude mode image (Fig 17 b) helped to study the sharp boundaries between the layers as well as some particles.

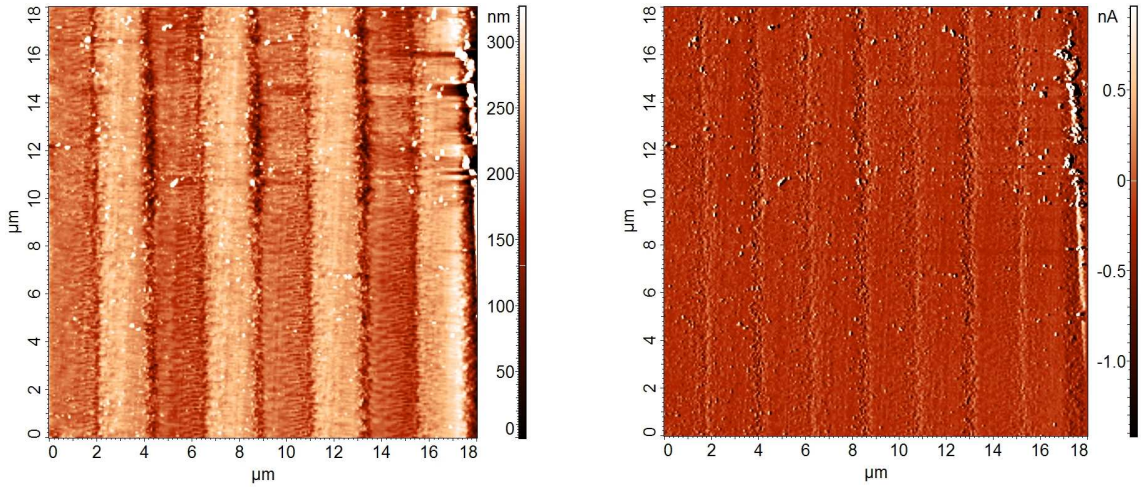

(a) (b)

Fig. 17 Non-contact mode AFM surface morphology of sectioned 10-layered a-SiC:H film (a) Topography height image, (b) Magnitude image.

The 3D view of individual layers gives the clear idea about the multilayer structure. The alternative layers 1, 3, 5, 7, 9 and the buffer layer were prepared at higher RF-power (10 W) and having the higher mechanical properties, were squeezed up. The layers of lower mechanical properties such as 2, 4, 6, 8, and 10 were, squeezed down.

The dispersion of the refractive index of each individual layers in multilayer (a-SiC:H) films was well corresponds to particular single layer film and thus, It was expected that the mechanical constants of individual layer were similar to particular single layer films.

The mechanical properties of each individual layers were characterized by nanoindentation method. The mean value of Young's modulus and hardness of individual layers are mentioned in Table 9. As mentioned previously, the individual layers in multilayered film were deposited of thickness of 100 nm and, hence the mechanical properties of them were measured until the contact depth of 30 to 40 nm, only. The obtained data were found to be similar to particular single layer films (A & B) as mentioned in Table 8. The 1st individual layer was not possible to characterized by nanoindentation technique due to the sharp cut was produced by sectioning method. The influence of substrate was observed on mechanical properties measurement, as the nanoindentation experiment was carried out from layer -2 to towards buffer layer.

Layers	Contact Depth (nm)	Young's modulus (GPa)	Hardness (GPa)
Layer – 2	42.53	12.7	1.12
Layer – 3	32.85	16.7	1.56
Layer – 4	38.74	13.1	1.28
Layer – 5	34.14	17.7	1.51
Layer – 6	38.26	14.8	1.32
Layer – 7	31.18	19.7	1.66
Layer – 8	37.43	15.8	1.365
Layer – 9	29.13	21.9	1.76
Layer – 10	33.15	17.9	1.56
Buffer layer	27.72	25.8	1.82

Table 9 Mechanical properties of individual layers of a-SiC:H multilayer film

4.4.3 Multilayer film analysis by Lateral Force Microscopy (LFM)

The friction characteristic of uncovered layers of the multilayer a-SiC:H film was analyzed by the help of the Lateral Force (LF) Microscopy. There is no friction coefficient difference observed between the layers, in spite of having different mechanical properties. This is due to the multilayer a-SiC:H film was deposited from the same monomer composition with only the changes of RF-power. Hence, the layers were having same friction coefficient.

4.4.4 Multilayer film analysis by Atomic Force Acoustic Microscopy (AFAM)

Further, the modulus mapping of multilayer a-SiC:H film was carried out by AFAM method. The AFAM is a newly developed non-destructive technique, used for the modulus mapping of thin films or polymers. The topographic image of multilayer structure in contact mode is mentioned in Fig 18 (a), while the AFAM image was produced at constant resonant phase (90.4^0 for the a-SiC:H multilayer film) is mentioned in Fig 18 (b). The frequency variation of the vibrated surface was scanned via phase modulation. In the AFAM image, the regions of the sample with lower stiffness are darker [22]. We observed that the spatial variation in the AFAM and conventional AFM images are identical, hence surface morphology of layer structure has no influence on mechanical property mapping.

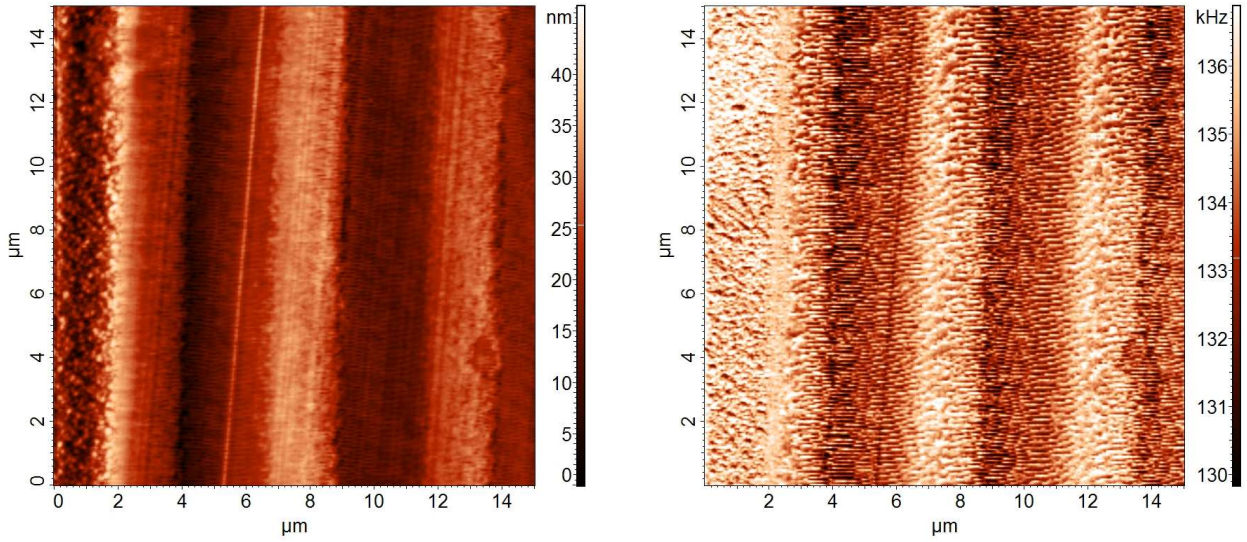

(a) (b)

Fig. 18 AFAM images of the sectioned a-SiC:H multilayer film. (a) topography, (b) AFAM frequency contrast.

5 CONCLUSION

Plasma-polymerized single and multilayer organosilicon films were deposited on silicon wafers using plasma-enhanced chemical vapor deposition. The study of surface properties and adhesion characteristics of these films were analyzed successfully by scanning probe microscopy, nanoindentation and nanoscratch tests.

The surface morphology and RMS roughness of single layer pp-VTES and pp-TVS films were successfully characterized by atomic force microscopy. The single layer pp-VTES films with thickness ranging from 15 nm to 8.6 µm were deposited at an effective power of 5 W. The RMS roughness was increased from 0.04 to 15.5 nm as a function of film thickness for pp-VTES films. In another experiment, single layer pp-TVS films were deposited at different RF-power of 10, 25, 50 and 70 W with the similar film thickness of about 1 µm. The RMS roughness was also increased from 1.90 to 4.0 nm for pp-TVS films as a function of different deposition power.

Mechanical properties of single layer pp-TVS films were measured using nanoindentation technique in 2 experimental set-ups. The 1st experimental set up was carried out at drift rate of ≤ 0.5 nm/s, while the 2nd set was carried out at a lower drift rate of ≤ 0.05 nm/s.

In the 1st experimental set up, the mechanical properties of the single layer pp-TVS film deposited at 10 W was used for analysis. we found out that the dwell time and loading/unloading times >5 s produced a progressive increase of the tip displacement likely due to a high system drift (<0.5 nm/s) not being correctly subtracted at prolonged measuring times. The increased tip displacement at prolonged measuring times resulted in underestimation of the Young's modulus and hardness. Thus, the cyclic nanoindentation using only 7 cycles during 90 s (measuring time) gave unsatisfying results.

The 2nd experimental set up was carried out for pp-TVS films deposited on silicon wafers by PECVD at three different powers (0.1, 2.5, and 10 W). All the films were characterized by conventional and cyclic nanoindentation methods under the drift rate ≤0.05 nm/s to construct the depth profile of mechanical properties. We found out that both the methods gave similar results but the cyclic nanoindentation accelerates depth analysis of mechanical properties significantly from hours using conventional method to minutes. The films of thickness about 1 µm were characterized for contact depth ranging from 5 to almost 200 nm. The Young's modulus and hardness data were reproducible, except for surface region up to 30 nm from the film surface, depending on film stiffness. Bulk reproducible data enabled to evaluate the Young's modulus and hardness of pp-TVS film deposited at different power: E=7.9 GPa, H=0.69 GPa (0.1 W), E=14 GPa, H=2.0 GPa (2.5 W), and E=17 GPa, H=3.0 GPa (10 W). The depth profiles of mechanical properties for films of different stiffness revealed that the 10% rule can be applied reliably to evaluate the hardness of film, but in case of Young's modulus, the rule cannot be used for stiffer film (E>14 GPa) deposited on silicon wafer. Based on this study, we can complete conditions necessary for successful analysis of mechanical properties at a shallow depth: (i) sharp indenter,

(ii) careful calibration of the indenter area function, (iii) minimal system drift and using drift correction, (iv) smooth sample, (v) no pile-up, and (vi) stiffer sample.

Further, hybrid nature of single layer pp-TVS films was investigated. The pp-TVS films deposited by PECVD with film thickness of 1 µm at different effective power, ranging from 10 – 70 W. Surface analysis (AFM) revealed grain structure of pp-TVS films deposited at different RF power. The RMS roughness and average grain size were increased from 3.4 nm to 21 nm and 29 nm to 241 nm, respectively with enhanced power. Nanoindentation measurements into the plane area and grains resulted in different depth profile of mechanical parameters. The difference was explained by influence of grain geometry and by lower mechanical parameters of grains with respect to the smooth area as confirmed by FEA simulation and AFAM measurements.

The adhesion behavior of single layer pp-TVS films on silicon substrates were tested by nanoscratch test and the surface morphology of scratches was examined by AFM. The correlation of both methods was informative. The different scratch speed experiment indicated that critical normal load was almost remained constant at different speed. The PECVD apparatus can reproducibly prepare the thin films with same adhesion characteristic. The different film thickness (thickness varying from 25 to 468 nm) has a great impact on adhesion behavior of the films. Similar way, the film of different mechanical properties (deposited from 10 – 70 W) had different adhesion behavior. The critical normal load and lateral normal load was increased with increased RF power from 10 to 50 W. However, the subsequent decline in scratch data (critical normal load, critical lateral load) was observed for film deposited at 70 W, probably due to the high internal stress and fragility. One can successfully use the nanoscratch test with the combination of atomic force microscopy in the evaluation of adhesion behavior of organosilicon thin films on silicon substrate.

Furthermore, a novel approached was discussed for the surface analysis of multilayer film. For that purpose, single layer and multilayered a-SiC:H films were deposited on silicon substrate from tetravinylsilane using PECVD. The multilayer film was sectioned using ultramicrotomy at an angle of 4° to reveal the individual layers. The individual layers were observed by atomic force microscopy and the surface morphology influenced by layer structure was noticed. There was no difference in friction characteristic of individual layers observed by lateral force microscopy. The mechanical properties of distinguished individual layers were successfully investigated by nanoindentation and atomic force acoustic microscopy. The analysis indicated that mechanical properties of individual layers A and B were the same in single layer and multilayer films. The results enable us construction of functional multilayered films of controlled mechanical properties applicable in polymer composites with controlled interphases.

REFERENCES

[1] T. Steiner, “Semiconductor Nanostructures for Optoelectronic Applications”, Arctech house, NorWood, MA (2004).
[2] B. Bhushan, “Handbook of Nanotechnology”, Springer, Heidelberg (2004).
[3] B. Bhushan, “Handbook of Micro/Nanotribology”, CRC Press, Boca Raton, Florida (1999).
[4] V.L. Mironov, “Fundamental of Scanning Probe Microscopy”, Russian Academy of Sciences, Nizhniy Novgorod (2004).
[5] W.C. Oliver, G.M. Pharr, J. Mater. Res. 7 (1992) 1564.
[6] C.C. Broomell, M.A. Mattoni, F.W. Zok, J.H. Waite, J. Exp Biol 209 (2006) 3129.
[7] Hysitron Triboscope user Manual (software version 8.0).
[8] V. Cech, L. Xu, J. Vanek, L.T. Drzal, Japanese J. of Appl. Phys. 45 (2006) 8440.
[9] R. Trivedi, V. Cech, *Proc. 5th Int. Symp. Juniormat*, Brno (2007) 121.
[10] V. Cech, in: S. Zhang (Ed.), Nanostructured Thin Films and Coatings, Volume 1, CRC Press, New York, 2010, pp. 481.
[11] R. Trivedi, V. Cech, Surf. Coat. Technol. (2010), doi:10.1016/j.surfcoat.2010.08.002.
[12] R. Cooper, Hysitron Inc. (private communication).
[13] A.C. Fischer-Cripss, The IBIS handbook of nanoindentation, Fischer-Cripps Laboratories, Forestville, 2005, p. 42.
[14] V. Cech, J. Studynka, N. Conte, V. Perina, Surf. Coat. Technol. 201 (2007) 5512.
[15] K.W. Lee, Y.-W. Chung, C.Y. Chan, I. Bello, S.T. Lee, A. Karimi, J. Patscheider, M.P. Delplancke-Ogletree, D. Yang, B. Boyce, T. Buchheit, Surf. Coat. Technol. 168 (2003) 57.
[16] P.S. Baker, Thin Solid Films 308-309 (1997) 289.
[17] K.W. Elhaney, J.J. Vlassak, W.D. Nix, J. Mater. Res. 13 (1998) 1300.
[18] R. Prikryl, V. Cech, P. Hedbavny, N. Inagaki, *Proc. 17th Int. Symp*, Plasma Chemistry, Toronto (2005) 1.
[19] R. Messier, J. Vac. Sci. Technol. A4 (1986) 490.
[20] W. Tang, K. Xu, J. Mater. Sci. Technol. 20 (2004) 78.
[21] Li R., Wadsworth I., Young J., Acheson R., J. Microscopy 184 (1996) 62.
[22] U. Rabe, S. Amelio, E. Kester, V. Scherer, S. Hirsekorn, W. Arnold, J. Ultrasonics 38 (2000) 430.